Dynamics of Scroll Waves of Excitation in a Mathematical Model of Ischaemic Border Zone

Irina V Biktasheva[1], Narine A Sarvazyan[2], Vadim N Biktashev[3]

[1] University of Liverpool, Liverpool, UK
[2] The George Washington University, Washington DC, USA
[3] University of Exeter, Exeter, UK

Abstract

Abnormal electrical activity from ischaemic boundary is one of major causes of ischemia-reperfusion arrhythmias, though exact mechanisms remain poorly understood. We used asymptotic theory of spiral waves drift based on response functions to compute specific forces acting on scroll waves in the vicinity of ischaemic border. The model included macroscopic gradients of cell-to-cell coupling and of cell excitability, and microscopic heterogeneity of individual cells, with Beeler-Reuter-Pumir explicit, albeit simplified, description of ionic currents. The quantitative interplay of specific forces explained formation of vortices, their drift together with recovering boundary, transient pinning to local inhomogeneities followed by penetration into bulk of healthy tissue. Likelihood of vortex escape into better coupled tissue depended on the border zone recovery speed. Direct numerical simulations confirmed the theoretical predictions for evolution of vortices.

1. Introduction

Reperfusion arrhythmias are associated with cardiac tissue recovery from acute ischemia, which can be more dangerous than ischemia itself, often leading to ventricular fibrillation and sudden cardiac death [1]. In a thin layer of cells sandwiched between intact healthy tissue and recovering ischaemic areas, Figure 1, rotating excitation waves can occur on a much smaller spatial scale compared to classical cardiac reentry [2]. Myocytes within such layers can become spontaneously active due to calcium overload and/or local noradrenaline release. The impact of intrinsic myocyte heterogeneity on network behaviour is enhanced by decrease in electrical coupling between the cells. It gets even more complicated as the physicochemical factors that create the boundary move in space due to dynamic nature of reperfusion [3]. The speed of retracting ischaemic border can vary in a rather wide range depending on reperfusion type, as blood flow can recover within

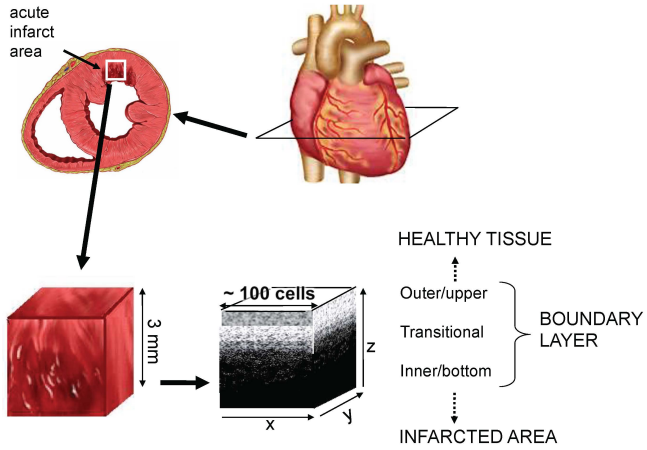

Figure 1. Excitation dynamics on a microscopic spatial scale.

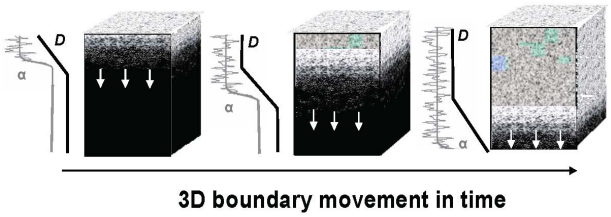

Figure 2. Distribution of diffusivity D and excitability α across the border zone moving downwards.

seconds (resolved coronary spasm, spontaneous dislodging of thrombi, angioplasty) or within minutes, if changes are due to gradual accumulation of metabolites or pharmacological interventions.

We used the asymptotic theory of spiral waves' drift and their response functions [4, 5] to obtain quantitative predictions for specific forces and corresponding drift velocities caused by recovering ischaemic border zone. The drift velocities explained experimental observation of rotating waves dragged together with the moving border zone, elucidated mechanisms of "pinning" to clusters of cells of

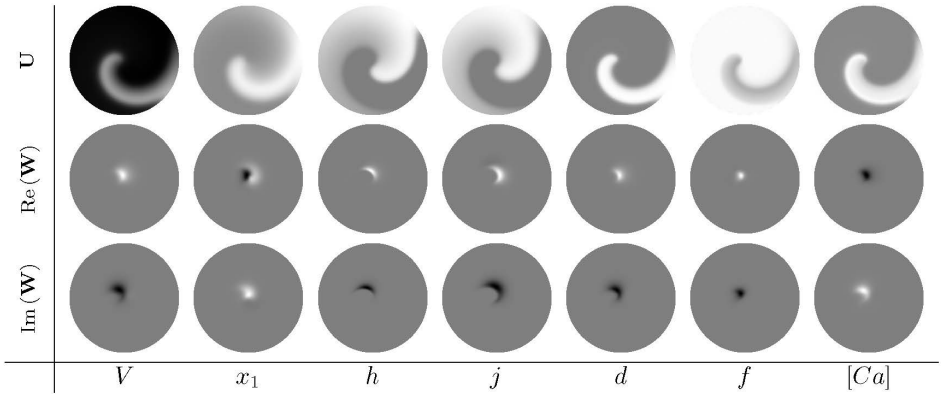

Figure 3. Spiral wave solution $\mathbf{U}$ and its translational response function $\mathbf{W}$, $\alpha = 0.115$. White corresponds to a value A and black to $-A$ chosen individually for each plot. The grey periphery of $\mathbf{W}$ plots corresponds to 0.

either elevated or suppressed excitability, as well as the mechanism by which pinning can give way to further drift. We confirmed the theoretical predictions by direct numerical simulations.

2. Methods

We modelled tissue recovering from acute ischaemia as a three-layered slab, Figure 2, of heterogeneous cells with modified Beeler-Reuter-Pumir [2, 6] (BRP) kinetics and moving vertical gradients of average cell excitability $\overline{\alpha}(z,t) > 0$ and of cell-to-cell coupling strength $D(z,t)$,

$$\begin{aligned}
\dot{V} &= -(1/C_m)(i_{K_1} + i_{x_1} + i_{Na} + i_s) + I_{ext},\\
i_{K_1} &= g_{K_1} \times \\
&\quad \left[\frac{4\,\mathrm{e}^{0.04(\mathrm{V}+85)} - 1}{\mathrm{e}^{0.08(\mathrm{V}+53)} + \mathrm{e}^{0.04(\mathrm{V}+53)}} + \frac{0.2(V+23)}{1-\mathrm{e}^{-0.04(\mathrm{V}+23)}}\right],\\
g_{K_1} &= 0.35(0.3 - \alpha(x,y,z,t)),\\
I_{ext} &= \nabla\left(D(z,t)\nabla V\right). \qquad (1)
\end{aligned}$$

Permeabilities of main currents were reduced vs the original Beeler-Reuter model: fast inward g_{Na} to 60% (2.4 vs 4), slow inward g_s to 50% (0.045 vs 0.09). In the inner layer, outward potassium rectifier g_{K_1}; was supressed to 30% of the standard value ($\alpha = 0$). At higher values of α, in upper layers, cells became automatic [6], Heterogeneity of excitability was described as

$$\alpha(x,y,z,t) = \overline{\alpha}(z,t)\,(1 + \delta_\alpha \eta(x,y,z)),$$

$\eta(x,y,z)$ was Gaussian uncorrelated random variable with unit dispersion, δ_α was the intensity of heterogeneity. Space-time variations of D and $\overline{\alpha}$ were defined as

$$\begin{aligned}
D(z,t) &= \begin{cases} D_{\min}, & z \le z_1,\\ D_{\min}^{\frac{z_2-z}{z_2-z_1}}\, D_{\max}^{\frac{z-z_1}{z_2-z_1}}, & z_1 \le z \le z_2,\\ D_{\max}, & z \ge z_2, \end{cases}\\
\overline{\alpha}(z,t) &= \frac{1}{2}\left(1 + \tanh\left(\frac{z-z_1}{w}\right)\right)\alpha_{\max}.
\end{aligned}$$

$z_1(t) = z_{1,0} - ct$ and $z_2(t) = z_{2,0} - ct$ were limits of the steepest part of coupling gradient, $w = 3 \times 30\mu\mathrm{m}$ was border zone width. In the inner layer, low excitability and weak coupling produced quiescent state with no wave propagation possible. In the outer layer, high excitability and strong coupling resulted in quiescent state capable to support wave propagation. In the middle layer, high excitability and weak coupling generated spontaneous fragmented waves. The layers moved downwards due washout of agents affecting the relevant tissue properties.

In absence of perturbation, *e.g.* heterogeneities and gradients, the asymptotic theory [4, 5] assumes stationary rotating spiral wave solution to (1),

$$\mathbf{u}(\vec{r},t) = \mathbf{U}(\rho(\vec{r}-\vec{R}), \vartheta(\vec{r}-\vec{R}) + \omega t - \Phi), \qquad (2)$$

with angular velocity ω, fiducial phase Φ; $\rho(\vec{r}-\vec{R}), \vartheta(\vec{r}-\vec{R})$ are polar coordinates centered at rotation center $\vec{R} = (X, Z)$. BRP model has stationary spirals for all α considered.

Perturbed spiral preserves the pattern and slowly drifts its core location and fiducial phase. It behaves as a localised object, only sensitive to perturbations affecting the core, due to localization of its response functions (RFs) in the vicinity of the core. The RFs are calculated numerically [5] together with the spiral wave solution (2).

Drift velocity is proportional to "*specific force*" γ caused by a perturbation $\mathbf{h}$,

$$\dot{R} \approx \epsilon\gamma = \epsilon \int_{\phi-\pi}^{\phi+\pi} e^{-\mathrm{i}\xi} \left\langle \mathbf{W}\,,\, \tilde{\mathbf{h}}(\mathbf{U};\rho,\theta,\xi)\right\rangle \frac{\mathrm{d}\xi}{2\pi}, \qquad (3)$$

where $\epsilon \ll 1$, $R = X + \mathrm{i}\,Z$; $\langle\cdot\,,\,\cdot\rangle$ stands for scalar product in functional space; $\tilde{\mathbf{h}}$ is the perturbation in the $\vec{R}$-centered corotating frame of reference (ρ,θ), $\theta = \vartheta + \omega t - \Phi(t)$ and $\phi = \omega t - \Phi(t)$. The kernel $\mathbf{W}(\rho,\theta) \in \mathbb{C}$ in (3) is the (translational) response function of the unperturbed spiral

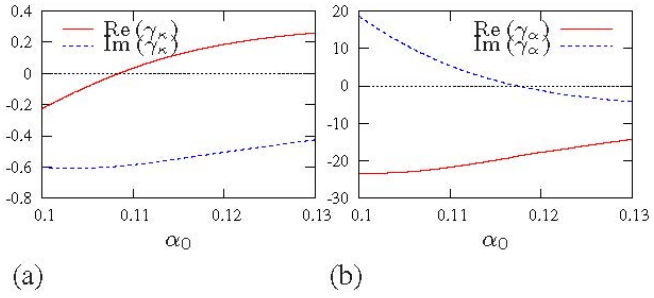

Figure 4. $D = 10^{-2}\,\mathrm{cm}^2/\mathrm{s}$. (a) Specific force γ_κ. (b) Specific force γ_α. Red solid lines: real parts, the longitudinal components. Dashed blue lines: imaginary parts, the lateral components.

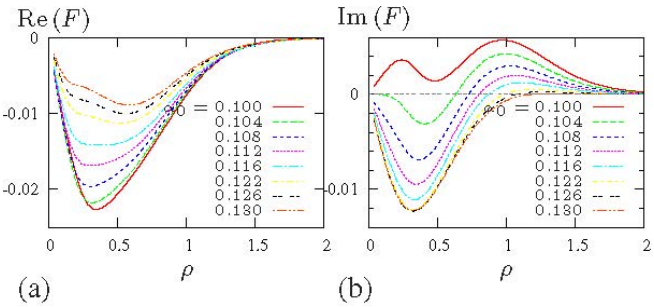

Figure 5. Specific force $\gamma_i = -\frac{R-r_c}{|R-r_c|}F(|R-r_c|)$. Dependence of (a) radial and (b) tangential components on the distance between spiral rotation centre R and inhomogeneity centre r_c, at selected values of background excitability α_0.

wave solution (2). The overall drift velocity is given by *superposition principle* as a sum of specific forces,

$$\dot{R} \approx \sum_j \gamma_j \epsilon_j,$$

here ϵ_j is magnitude of j-th perturbation, and γ_j is the specific force produced by a unit perturbation of that sort.

In our model, the specific forces were: γ_κ caused by the filament curvature, γ_i and γ_α caused by localised inhomogeneities and smooth gradient of parameter α respectively, and γ_D caused by gradient of diffusivity. Note that $\gamma_D = -\gamma_\kappa$ [2, 7]. The real component $\mathrm{Re}\,(\gamma_\kappa)$, also called *filament tension* b_2, has special importance. If $\mathrm{Re}\,(\gamma_\kappa) = b_2 > 0$, a ring filament collapses, if $b_2 < 0$, filament grows leading to fibrillation like "turbulence" [8,9]. $\mathrm{Re}\,(\gamma_\alpha)$ is the component γ_α along gradient of α and is positive if the drift is towards higher values of α. Radial component $\mathrm{Re}\,(F)$ of the specific force γ_i is positive if the spiral moves towards the inhomogeneity centre [5, 10]

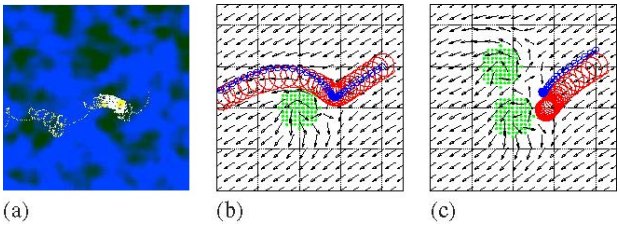

Figure 6. (a) Temporary pinning to high-α cluster. The colour background shows distribution of $\eta(x,y)$, smoothened by sliding averaging, (greenish) dark corresponds to high α and (blue) light to low α. (b) Drift around a repelling inhomogeneity (green dots). $\alpha = 0.13$ in the bulk of the medium and $\alpha = 0.15$ within inhomogeneity. Red solid line is the tip trajectory. Arrows show predicted velocity field (3). Small blue open circles show predicted instant centres of rotation corresponding to one rotation period. (c) Two repelling inhomogeneities of the same kind as in (b) can stop the drift altogether.

3. Results

Figure 3 shows density plots for a spiral wave and its translational response function in BRP model. Based on the RFs, Figure 4(a) shows theoretical prediction for the filament tension $b_2 = \mathrm{Re}\,(\gamma_\kappa)$ changing sign in the considered interval of parameter α. It also determines the drift component along gradient of diffusivity $\mathrm{Re}\,(\gamma_D) = -\mathrm{Re}\,(\gamma_\kappa) = -b_2$, and $\mathrm{Im}\,(\gamma_D) = -\mathrm{Im}\,(\gamma_\kappa) = -c_3$ across it. So, at higher values of α, negative $\mathrm{Re}\,(\gamma_D)$ must drag spirals towards poor coupled regions, while at lower α, positive $\mathrm{Re}\,(\gamma_D)$ must push spirals towards better coupled regions. Figure 4(b) shows theoretical prediction for drift due to smooth gradient of excitability α. $\mathrm{Re}\,(\gamma_\alpha)$ is negative in the whole range of α_0, so spirals should drift towards lower excitability, which agrees with the general rule noted *e.g.* in [11, 12].

Figure 5 shows theoretical prediction for spiral interaction with a point-like heterogeneity in parameter α. Here, $\mathrm{Re}\,(F(\rho)) < 0$ for all α and all distances ρ between the spiral and inhomogeneity, so spirals are attracted to spots of lowered excitability, $\epsilon_i < 0$, and vice versa. However, simulations showed pinning even to repelling spots [3] (Figure 6(a)). This be either temporary pinning (Figure 6(b)), or permanent pinning to a certain lay-out of repelling heterogeneities (Figure 6(c)).

Figure 7 shows two 3D simulations. At $\alpha = 0.105$, negative filament tension (cf Figure 4(a)) and repelling gradient of diffusivity allowed scrolls to penetrate into the bulk of the tissue, where they persisted after the ischaemic border zone had disappeared. At $\alpha = 0.115$, positive filament tension in the upper layer did not allow scrolls to grow, and the attractive gradient of diffusivity dragged them together

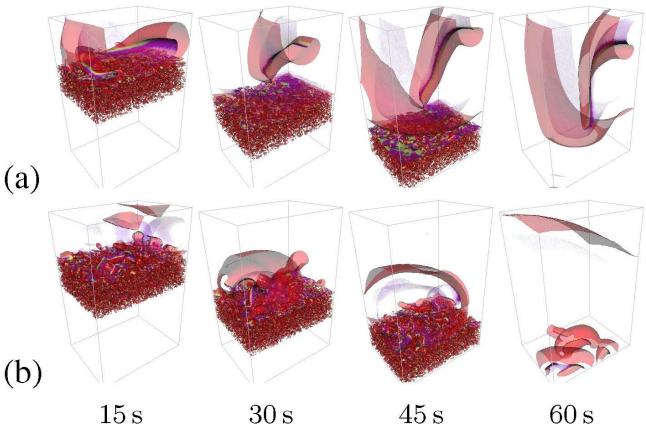

Figure 7. Vortex formation by moving border zone. $D_{\max} = 10^{-3}\,\mathrm{cm}^2/\mathrm{s}$, $\delta_\alpha = 0.5$, box size $120 \times 90 \times 180$ cells, border speed $c = 3\,\mathrm{cell}/\mathrm{s}$. (a) $\alpha_{\max} = 0.105$; (b) $\alpha_{\max} = 0.115$.

with the moving border zone. Continuation of the simulation Figure 7(b) led to complete elimination of all activity. All that was in full agreement with what could be expected from the asymptotic theory predictions.

4. Discussion

In this study, we considered the asymptotic theory's quantitative predictions for the forces causing drift of cardiac re-entry in the vicinity of ischaemic border zone. The predictions allowed to tell apart and highlight different mechanisms of arrythmogenesis by the ischaemic boder zone in three-dimentiontional settings. The direct numerical simulations with deliberately arranged conditions confirmed the theoretical predictions for the drift, and make predictions, not available from tissue culture experiments.

The drift and pinning of spirals are due to combination of the gradients of coupling and excitability, and microscopic heterogeneity of excitability. Pinning of spirals to heterogeneity, even if temporary, helps them to escape into the bulk of the tissue and produce macro-reentry, despite the smooth gradients. In three dimensions, the filament tension's effects enhance arrhythmogeneity if excitability in the bulk is low, or suppress it if the excitability is high.

In vivo, the above considered scenarios will be affected by multiple additional factors (excitability kinetics, presence of highly excitable Purkinje fibers, macroscopic myofiber orientation, coronary vessels, fibrous or fat deposits, transmural differences in myocytes metabolic activity and their sensitivity to ischaemia). Yet, with all its limitations, this study represents one of the first attempts to theoretically explore a very complex set of highly arrhythmogenic conditions that can occur on the boundary of the recovering ischaemic tissue.

Acknowledgments

This work was supported by EPSRC, UK (EP/D074789/1, EP/I029664/1). Experimental work that led to this study was supported by NIH (HL076722, HL095828). We are grateful to A. Arutunyan for experimental and conceptual input, and to D. Barkley, G. Bordyugov, A. Foulkes, A. Karpov and R. McFarlane for programming and numerical expertise contributions.

References

[1] Wit AL, Janse MJ. Reperfusion arrhythmias and sudden cardiac death: a century of progress toward an understanding of the mechanisms. Circulation Research 2001; 89(9):741–743.

[2] Biktashev VN, Biktasheva IV, Sarvazyan NA. Evolution of spiral and scroll waves of excitation in a mathematical model of ischaemic border zone. PLoS ONE 2011; 6(9):e24388.

[3] Biktashev VN, Arutunyan A, Sarvazyan NA. Generation and escape of local waves from the boundary of uncoupled cardiac tissue. Biophys J 2008;94:3726–3738.

[4] Biktasheva IV, Biktashev VN. On a wave-particle dualism of spiral waves dynamics. Phys Rev E 2003;67:026221.

[5] Biktasheva IV, Barkley D, Biktashev VN, Foulkes AJ. Computation of the drift velocity of spiral waves using response functions. Phys Rev E 2010;81(6):066202.

[6] Pumir A, Arutunyan A, Krinsky V, Sarvazyan N. Genesis of ectopic waves: role of coupling, automaticity, and heterogeneity. Biophys J 2005;89:2332–2349.

[7] Dierckx H, Bernus O, Verschelde H. A geometric theory for scroll wave filaments in anisotropic excitable media. Physica D 2009;238:941–950.

[8] Brazhnik PK, Davydov VA, Zykov VS, Mikhailov AS. Vortex rings in excitable media. Sov Phys JETP 1987;66:984.

[9] Biktashev VN. A three-dimensional autowave turbulence. Int J of Bifurcation and Chaos 1998;8(4):677–684.

[10] Biktashev VN, Barkley D, Biktasheva IV. Orbital movement of spiral waves. Phys Rev Lett 2010;104:058302.

[11] Rudenko AN, Panfilov AV. Drift and interaction of vortices in two-dimensional heterogeneous active medium. Studia Biophysica 1983;98(3):183–188.

[12] Ten Tusscher KHWJ, Panfilov AV. Reentry in heterogeneous cardiac tissue described by the Luo-Rudy ventricular action potential model. Am J Physiol Heart and Circ Physiol 2003;284(2):H542–H548.

Address for correspondence:

Irina V. Biktasheva
Department of Computer Science, Ashton building,
University of Liverpool, Liverpool L69 3BX, UK
ivb@liverpool.ac.uk